J Mater Sci: Mater Electron (2023) 34:223

Effects of Sn-Ag-x leveling layers on the microstructure and shear behavior of Sn-58Bi solder joint under thermal cycling

Huifeng Chen[1,2], Yang Liu[2,*], Shuang Zhang[3,4,*], Rongxing Cao[2], and Yuxiong Xue[2]

[1] College of Information Engineering, Yangzhou University, Yangzhou, China
[2] College of Electrical, Energy and Power Engineering, Yangzhou University, Yangzhou, China
[3] Flowmeter Branch, Chongqing Chuanyi Automation Co.,Ltd, Chongqing, China
[4] School of Material Science and Engineering, Harbin University of Science and Technology, Harbin, China

Received: 17 September 2022
Accepted: 17 November 2022
Published online: 20 January 2023

© The Author(s), under exclusive licence to Springer Science+Business Media, LLC, part of Springer Nature 2023

ABSTRACT

Four Sn-Ag-x (Sn-3.0Ag-0.5Cu, Sn-0.3Ag-0.7Cu, Sn-0.3Ag-0.7Cu-0.5Bi-0.05Ni, and Sn-3.0Ag-3.0Bi-3.0In) leveling layers were coated on Cu substrate to improve the reliability of Sn-58Bi (SnBi) solder joints under thermal cycling. The microstructure, interfacial intermetallic compounds (IMC), and shear behavior of the solder joints under thermal cycling conditions were investigated. The microstructure of the solder joint becomes coarsened after thermal cycling test. After 700 thermal cycles, the SnBi/Sn-Ag-x/Cu solder joint shows a more refined microstructure than the SnBi joint does. The interfacial IMC of SnBi/Cu solder joints and SnBi/Sn-Ag-x/Cu solder joints become thicker as the thermal cycle increases. However, the IMC growth rate of SnBi/Sn-Ag-x/Cu is significantly lower than that of SnBi/Cu. Meanwhile, the Sn-Ag-x leveling layers effectively suppress the growth of the Cu_3Sn IMC layer. The thermal cycling environment decreases the bonding strength of all solder joints. The shear strength of the SnBi/Sn-Ag-x/Cu solder joint is higher than that of SnBi/Cu under the same conditions. The brittle damage induced by the thermal cycling is suppressed by the addition of the Sn-Ag-x leveling layers.

1 Introduction

In recent years, advanced electronic products have shown explosive growth, and new electronic packaging technologies continue to emerge [1–3]. The reliability of lead-free solder joints is a key factor affecting the service life of electronic devices, and has always been a hot issue of research [4–6]. Among them, SnBi solder has attracted much attention in the field of low temperature packaging due to its low melting point and low cost [7, 8]. However, as the result of the high concentration of Bi, the ductility of

Address correspondence to E-mail: lyang805@163.com; zhangs2513@163.com

https://doi.org/10.1007/s10854-022-09590-y

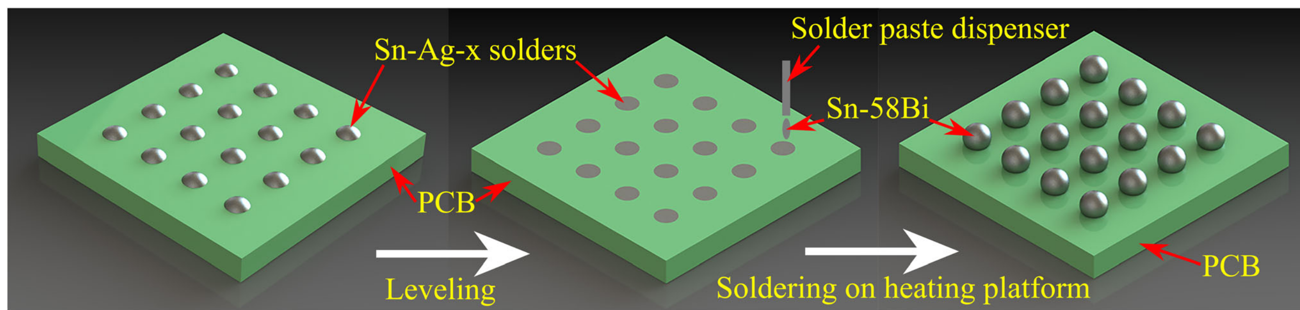

Fig. 1 Schematic diagram of solder joint preparation

solder joint is poor. Bi particles tend to aggregate to the interface during use, causing the mechanical properties of solder joints to decrease [9–11]. In addition, the development trend of miniaturization of electronic products has reduced the geometric size of solder joints. The influence of periodic changes at ambient temperature on the reliability of solder joints is also a factor that cannot be ignored [12]. Due to the difference in the coefficient of thermal expansion (CTE) between the substrate and the packaging material, stress will be generated at the joint between the solder joint and the substrate [13, 14]. With the continuous conversion of high and low temperatures, the microstructure and the interfacial IMC layer grow, which ultimately leads to a decrease in the mechanical properties of solder joints [5]. Therefore, improving the reliability of solder joints under thermal cycling is of great significance.

Thermal cycling is a commonly used accelerated test method to evaluate the reliability of electronic devices. Wang et al. [15] added Ce into the Sn-3.3Ag-0.2Cu-4.7Bi solder. When the added amount of Ce is 0.03 wt%, the growth rate of the interface IMC of the solder joint is the lowest during the thermal cycling of −55–125 °C. Miao et al. [16] found that the mechanical properties of SnBi-Cu solder joints are better than those of SnBi solder joints after 2000 thermal cycles, indicating that adding Cu to SnBi solder is beneficial to the reliability of solder joints. Research by Yang et al. [5] showed that the microstructure of SnBi solder joints has been refined due to the addition of nano-molybdenum particles. The shear strength and tensile properties of SnBi-0.25Mo solder joints are always higher than those of SnBi solder joints under different temperature cycles. In addition to adding components to the solder, it is also a feasible solution to optimize the performance of solder joints through the change of under bump metal (UBM). Since Sn-Ag-Cu alloy has better ductility than SnBi does [17], it can be used as an additive layer material between SnBi and the substrate. Wang et al. [18] found that Sn-3.0Ag-0.5Cu (SAC305) as a UBM layer can effectively improve the mechanical properties of SnBi solder during the aging process. Adding additive layer on the solder pad is a feasible solution to improve the reliability of solder joints under thermal cycling. Our previous research designed SnBi/Sn-Ag-x/Cu structure solder joints [19], and found that the addition of Sn-Ag-x leveling layer effectively improves the reliability of SnBi solder after isothermal aging. However, the performance and reliability of this structure under thermal cycling remain to be revealed.

To evaluate the effects of the Sn-Ag-x leveling layer on the reliability of SnBi solder joints under temperature cycling conditions, this paper fabricated Sn-Ag-x leveling layers on Cu substrate. The microstructure and interfacial IMC layer of the SnBi/Sn-Ag-x/Cu solder joints under thermal cycling were studied.

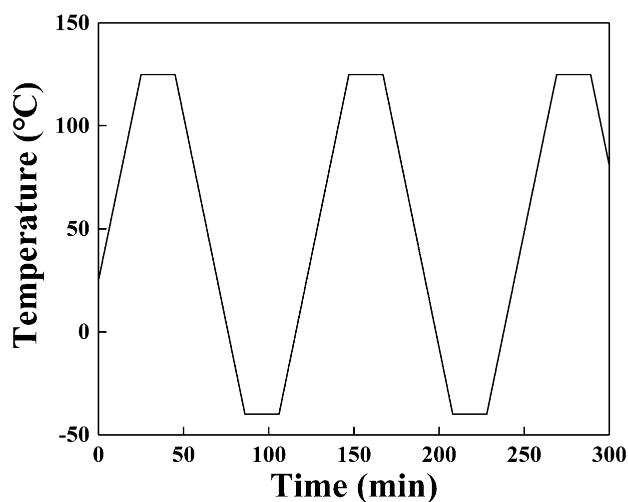

Fig. 2 Temperature curve of the thermal cycling process

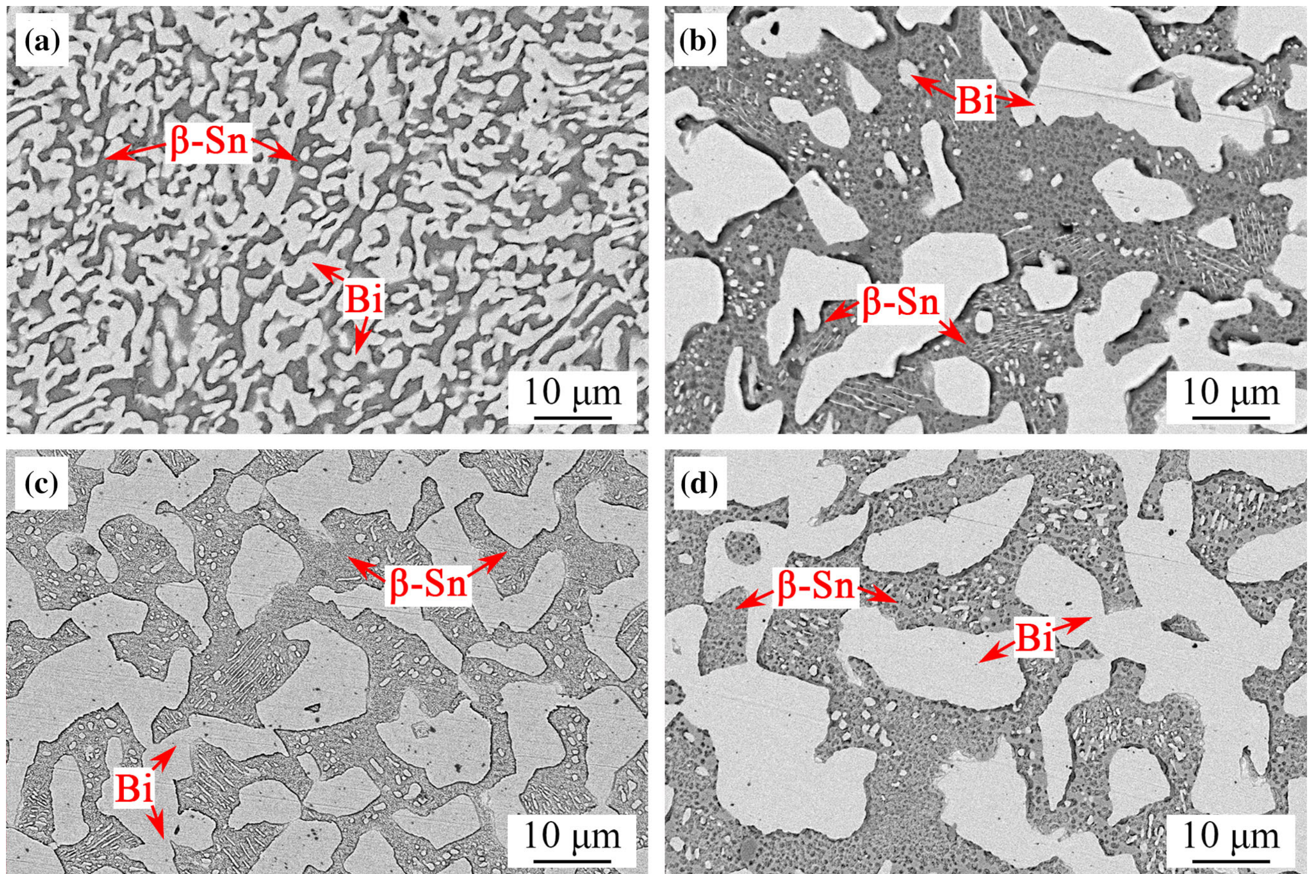

Fig. 3 Microstructure of SnBi/Cu solders after thermal cycling, **a** 0 cycles, **b** 300 cycles, **c** 500 cycles, and **d** 700 cycles

Meanwhile, the shear behavior of the solder joints was analyzed.

2 Experimental procedure

Commercial Sn-58Bi (SnBi), Sn-3.0Ag-0.5Cu (SAC305), Sn-0.3Ag-0.7Cu (SAC0307), Sn-0.3Ag-0.7Cu-0.5Bi-0.05Ni (SACBN), and Sn-3Ag-3Bi-3In (SABI333) pastes were used as the soldering materials in this study. The diameter of Cu pads on the printed circuit board (PCB) substrates was 680 μm. And the organic solderability preservative (OSP) treatment was conducted on those Cu pads to protect them from being oxidized. As shown in the schematic diagram in Fig. 1, SAC305, SAC0307, SACBN, SABI333 solder pastes were printed onto the pads, and then were soldered for 80 s on a heating platform. Among them, the soldering temperature of SAC305, SAC0307, and SACBN solder was 260 °C, and the heating temperature of SABI333 solder was 230 °C. The solder joints were ground and ultrasonically cleaned to obtain the prepared leveling layers. Subsequently, SnBi solder paste was printed onto the leveling layers and was soldered at 180 °C for 80 s to obtain the solder joints on different leveling layers.

Solder joints were tested with 300, 500 and 700 thermal cycles using a VT 4004 test chamber. According to the standard of JESD22-A104E, the temperature curve of this test is shown in Fig. 2. Here the test temperature is −40–125 °C, the heating and cooling rate is 4 °C/min, and the holding time is 20 min. The microstructure and interfacial IMC structure of the solder joints after thermal cycling were observed by scanning electron microscopy (SEM), and the compositions was analyzed by energy dispersive X-ray spectroscopy (EDS). The shear

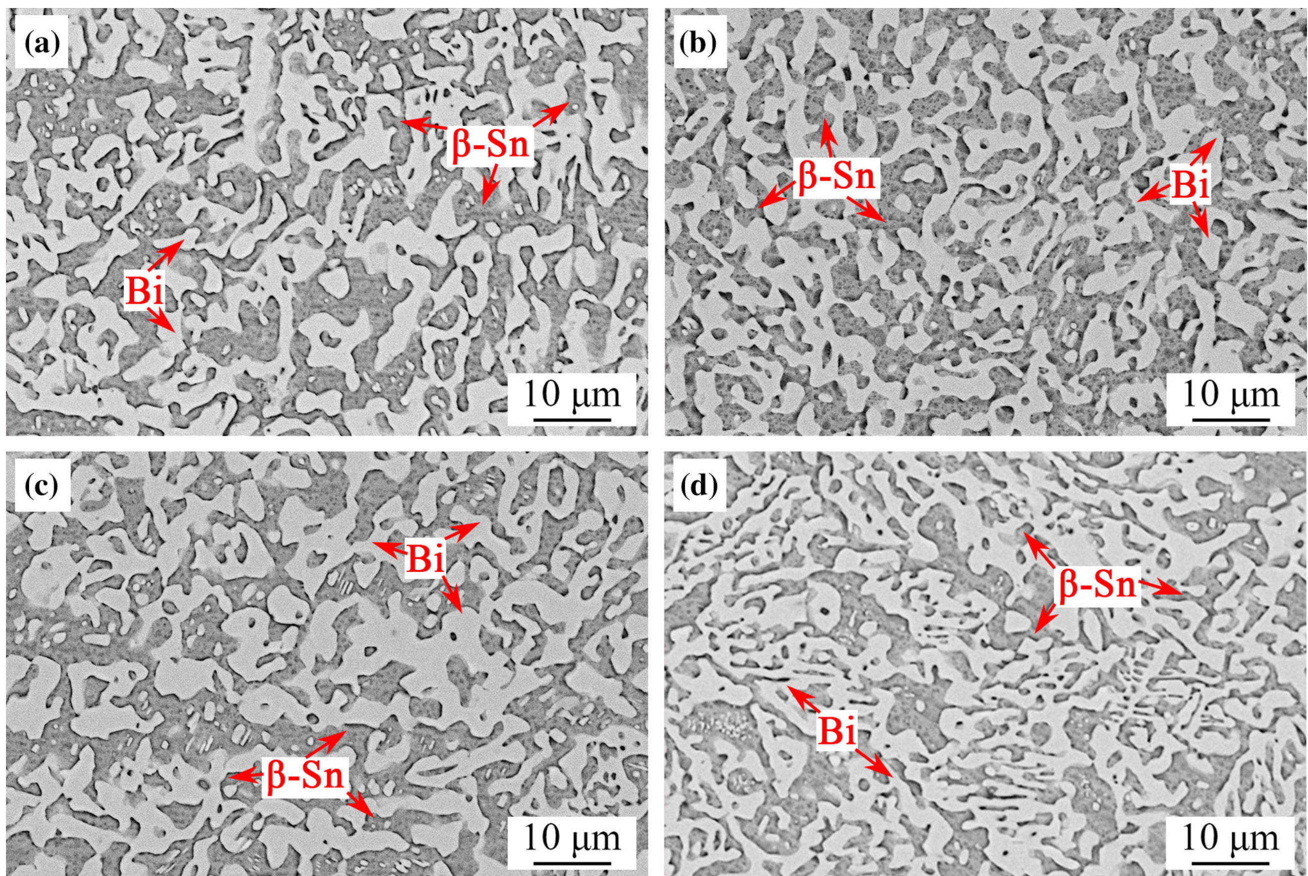

Fig. 4 Microstructure of SnBi/Sn-Ag-x/Cu solder joints, **a** SnBi/SAC305/Cu, **b** SnBi/SAC0307/Cu, **c** SnBi/SACBN/Cu, and **d** SnBi/SABI333/Cu

strength of the solder joints was tested using the RESCH PTR-1100 tester. The shear rate during the test was 0.02 mm/s and the shear height was 45 μm.

3 Results and discussion

3.1 Microstructure

Figure 3 represents the microstructure of SnBi/Cu solder joints after 0, 300, 500, and 700 thermal cycles, respectively. As shown in Fig. 3a, the Bi-rich phase and β-Sn phase are the main components of the microstructure of the SnBi solder joint. As shown in Fig. 3b–d, the microstructure of the solder joint is coarsened with the increasing cycles, and refined Bi-rich particles appear in the coarsened β-Sn block. The microstructure is coarsened after 300 cycles, while the growth rate of the microstructure decreases when the number of cycles reaches 500 and 700. In the high-temperature stage, the motion rates of Bi, Sn, and Cu atoms improve with the increasing temperature. This accelerates the movement between atoms, making each phase of the solder joint coarsened. When the temperature begins to drop, according to the Sn-Bi phase diagram, the solubility of Bi-rich in β-Sn decreases and the tiny Bi-rich grains precipitate from the β-Sn phase presented in the figure.

Figure 4 shows the microstructure of SnBi/Sn-Ag-x/Cu solder joints. Compared with SnBi/Cu solder joints, the proportion of β-Sn phase in the microstructure of SnBi/Sn-Ag-x/Cu solder joints significantly increases. The Sn-Ag-x solder leveling layer diffuses into the molten SnBi alloy during the secondary soldering process. This results in the transformation of the composition in the liquid SnBi alloy. The four solder alloys used as the leveling layer are all dominated by Sn. Therefore, the alloy composition of SnBi changes in the hypo-eutectic direction. During the solidification process of the alloy, β-Sn precipitates preferentially, and then the eutectic

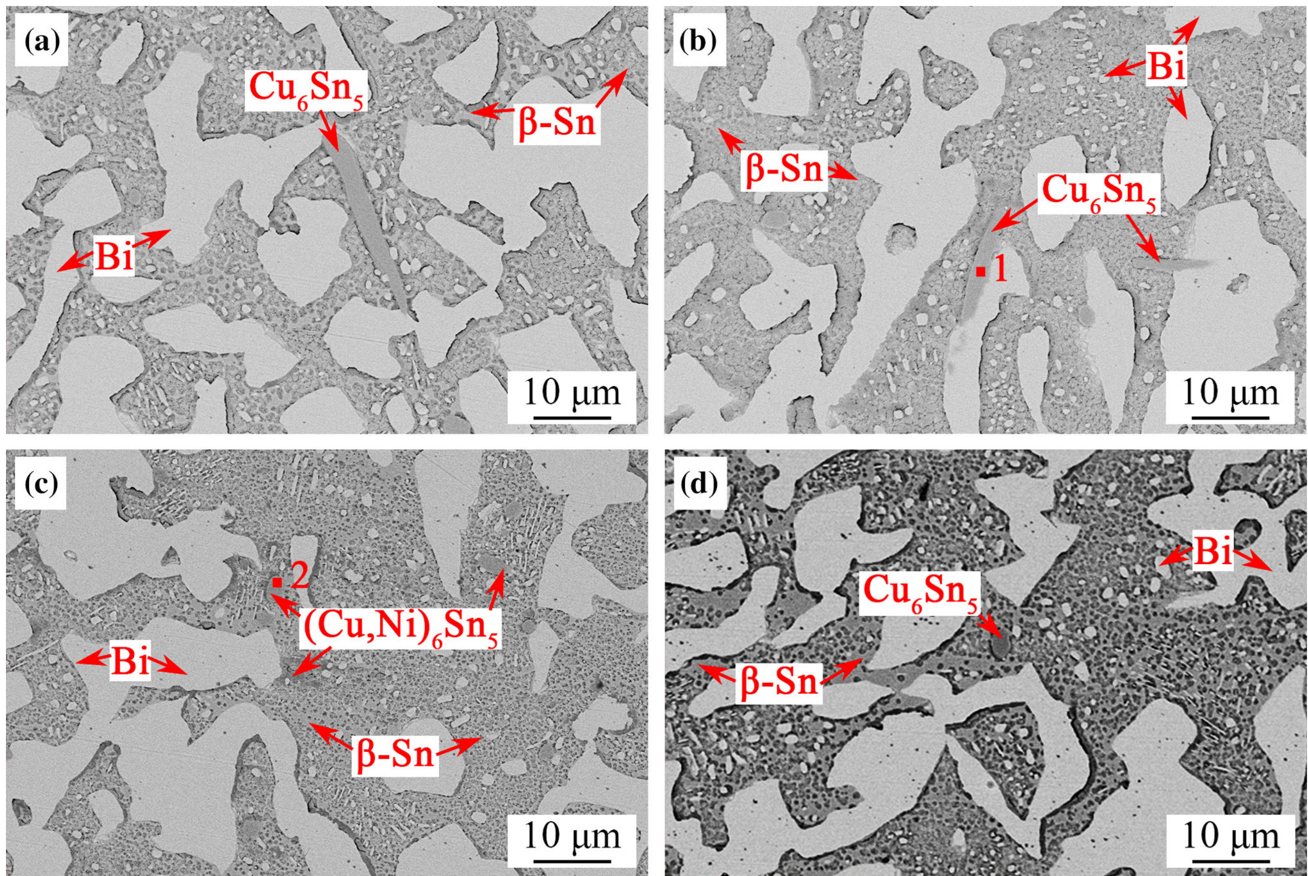

Fig. 5 Microstructure of SnBi/Sn-Ag-x/Cu solder joints after 700 thermal cycles, **a** SnBi/SAC305/Cu, **b** SnBi/SAC0307/Cu, **c** SnBi/SACBN/Cu, and **d** SnBi/SABI333/Cu

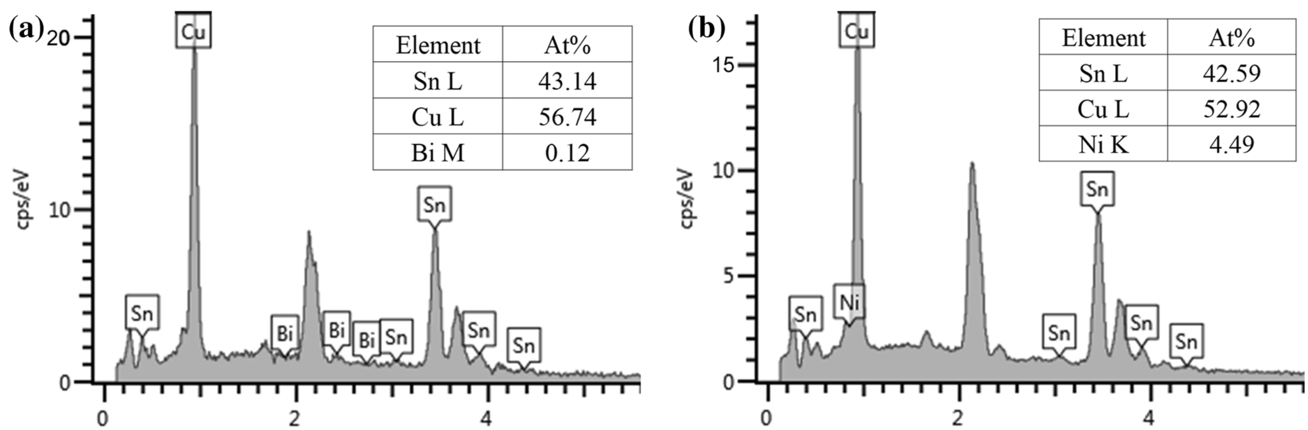

Element	At%
Sn L	43.14
Cu L	56.74
Bi M	0.12

Element	At%
Sn L	42.59
Cu L	52.92
Ni K	4.49

Fig. 6 **a** EDS of point 1 in Fig. 5 and **b** EDS of point 2 in Fig. 5

phase is formed. In contrast, the Sn content in SABI333 solder is lower, while the Bi content is higher than that of the other three kinds of solder. Therefore, the Bi-rich matrix in the welded microstructure is still relatively dense, and the grain size of the β-Sn phase is smaller than those of the other three solder joints.

Figure 5 shows the microstructure of SnBi/Sn-Ag-x/Cu solder joints after 700 thermal cycles. Like the change of SnBi/Cu solder joints, the phases in the

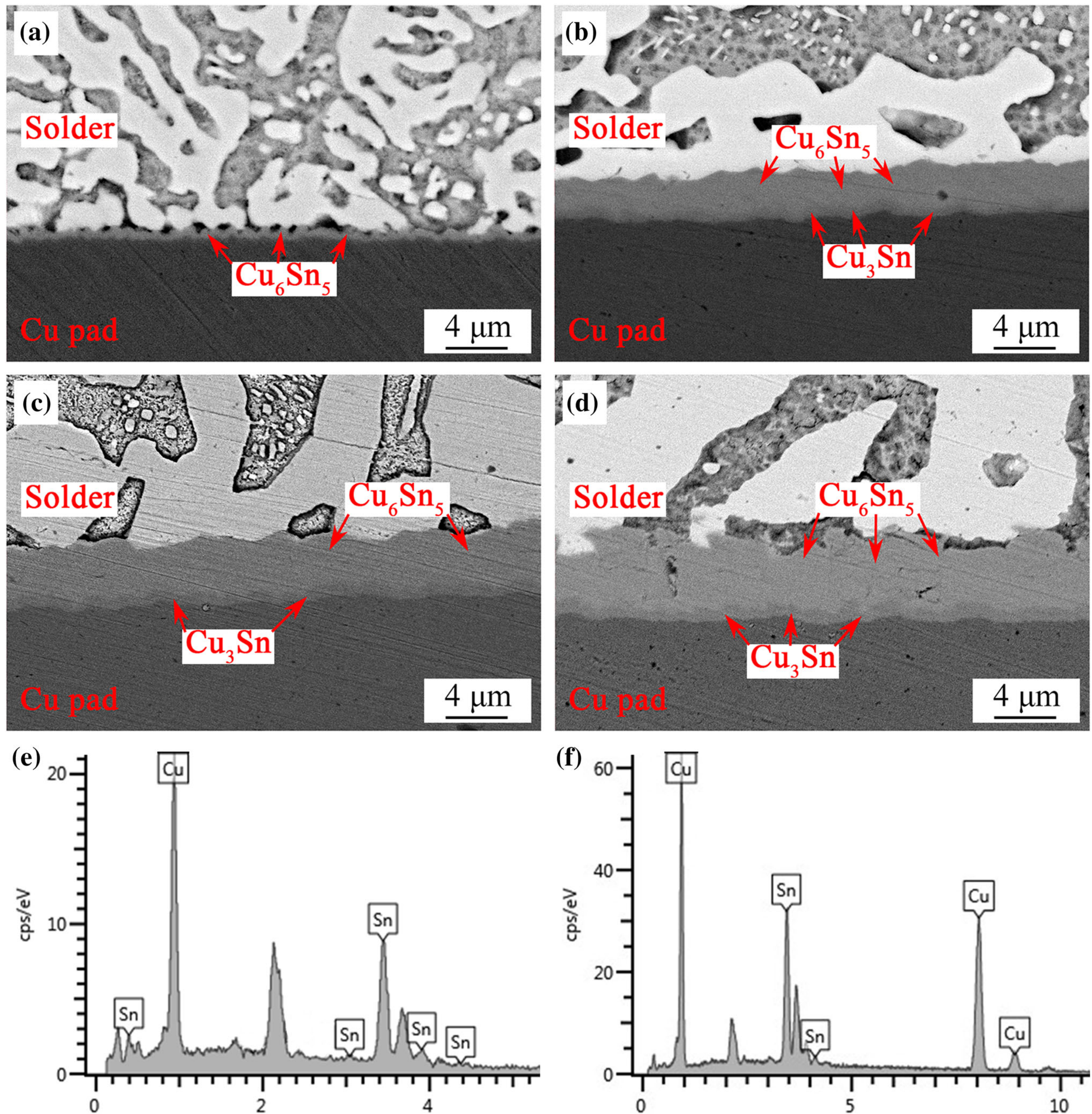

Fig. 7 IMC structure of interface after thermal cycling of SnBi/Cu solder joint, **a** 0 cycles, **b** 300 cycles, **c** 500 cycles, **d** 700 cycles, **e** EDS of Cu_6Sn_5, and **f** EDS of Cu_3Sn

microstructure gradually change from small particles to large blocks with thermal cycles increasing. In addition, rod-like IMCs are formed at the phase interface in the SnBi/Sn-Ag-x/Cu solder joints, which are confirmed as Cu_6Sn_5 and $(Cu, Ni)_6Sn_5$ by EDS in Fig. 6. Since the Sn-Ag-x leveling layers dissolve into SnBi solder, Cu_6Sn_5 phase formed by the reaction between Cu and Sn atoms disperses in the solder. The physical properties of the Ni element are similar to that of the Cu element which replaces part of Cu in Cu_6Sn_5 to form $(Cu, Ni)_6Sn_5$. In the high-temperature stage of the thermal cycling, Cu atoms in the substrate diffuse into the solder and react with Sn atoms continuously to form compounds. Due to the existence of IMC grains in the microstructure, the movement of grain boundaries is hindered, and the

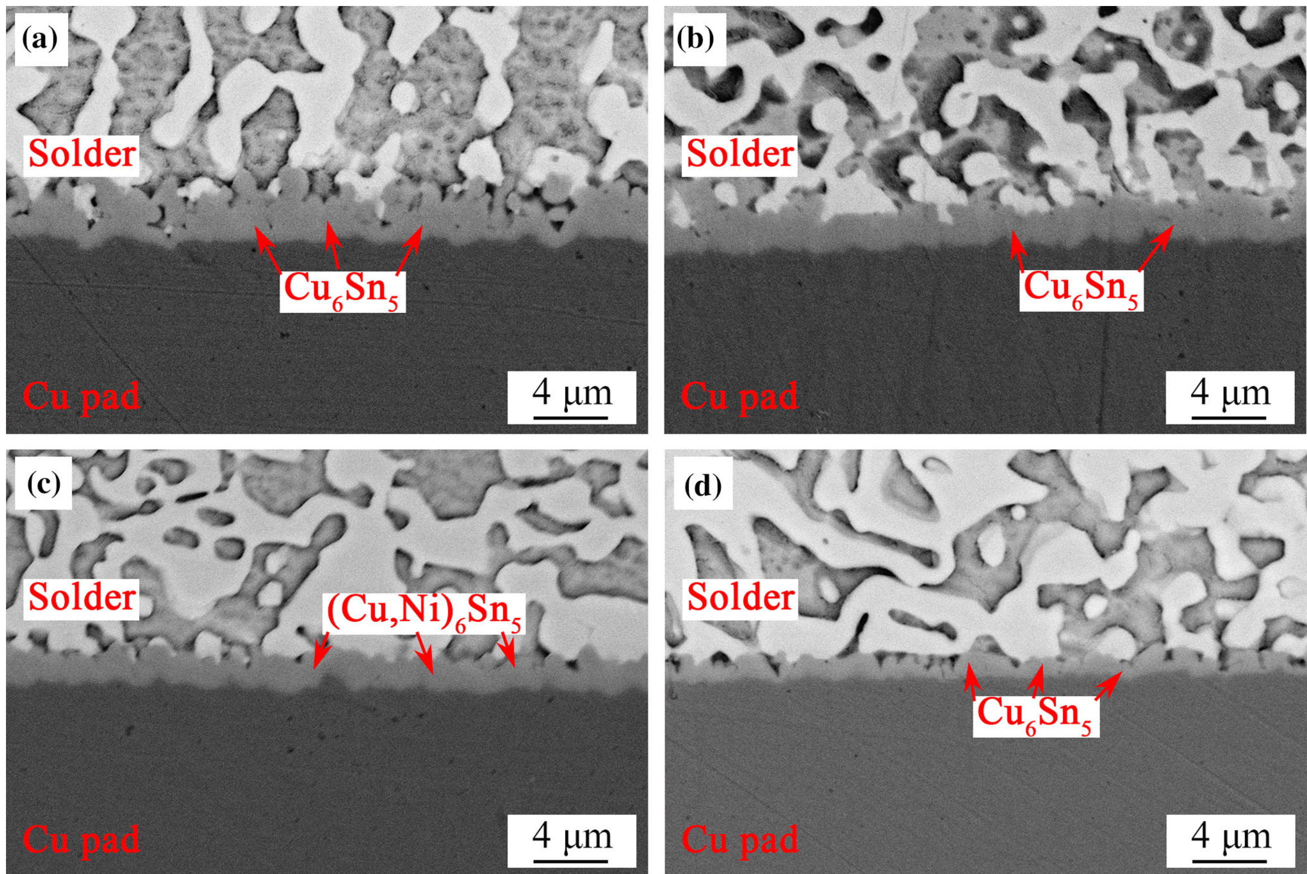

Fig. 8 The interface IMC morphology of the SnBi/Sn-Ag-x/Cu solder joints, **a** SnBi/SAC305/Cu, **b** SnBi/SAC0307/Cu, **c** SnBi/SACBN/Cu, and **d** SnBi/SABI333/Cu

precipitation and aggregation speed of Bi particles and Sn-rich phase is reduced. Therefore, compared to the SnBi/Cu solder in Fig. 3d, the microstructure of the SnBi/Sn-Ag-x/Cu solder joint after 700 thermal cycles is more refined.

3.2 Interfacial IMCs layer after thermal cycling

Figure 7 shows the IMC morphologies of SnBi/Cu solder joints after 0, 300, 500, and 700 thermal cycles. Before thermal cycling, the interfacial IMC shape of SnBi/Cu solder joints is scalloped, as shown in Fig. 7a. According to the reported study [20], the IMC layer formed by the metallurgical reaction between SnBi/Cu solder joints is mainly Cu_6Sn_5. Figure 7b–d show that the total thickness of the interfacial IMC increases with the increase of the number of thermal cycles, and the interface morphology gradually becomes smooth. On one hand, the growth of interfacial IMCs is mainly based on the element diffusion at the interface. The grain boundary position has higher energy, which is more likely to promote the nucleation and growth of IMC, causing the IMC layer to become smooth. In addition, the interfacial IMC is fractured due to thermal mismatch during temperature cycling, thereby increasing the number of grain boundaries and resulting in a smoother IMC layer after thermal cycling [21]. A discontinuous Cu_3Sn layer appears in the solder joints after 300 thermal cycles and a continuous Cu_3Sn layer with a certain thickness forms after 700 thermal cycles. The growth and formation of Cu_6Sn_5 and Cu_3Sn in the interfacial IMC follow the reactions below:

$$6Cu + 5Sn \rightarrow Cu_6Sn_5 \quad (1)$$

$$Cu_6Sn_5 + 9Cu \rightarrow 5Cu_3Sn \quad (2)$$

Cu_6Sn_5 IMC is formed by the reaction of Sn atoms with Cu atoms from Cu substrate. The formation and

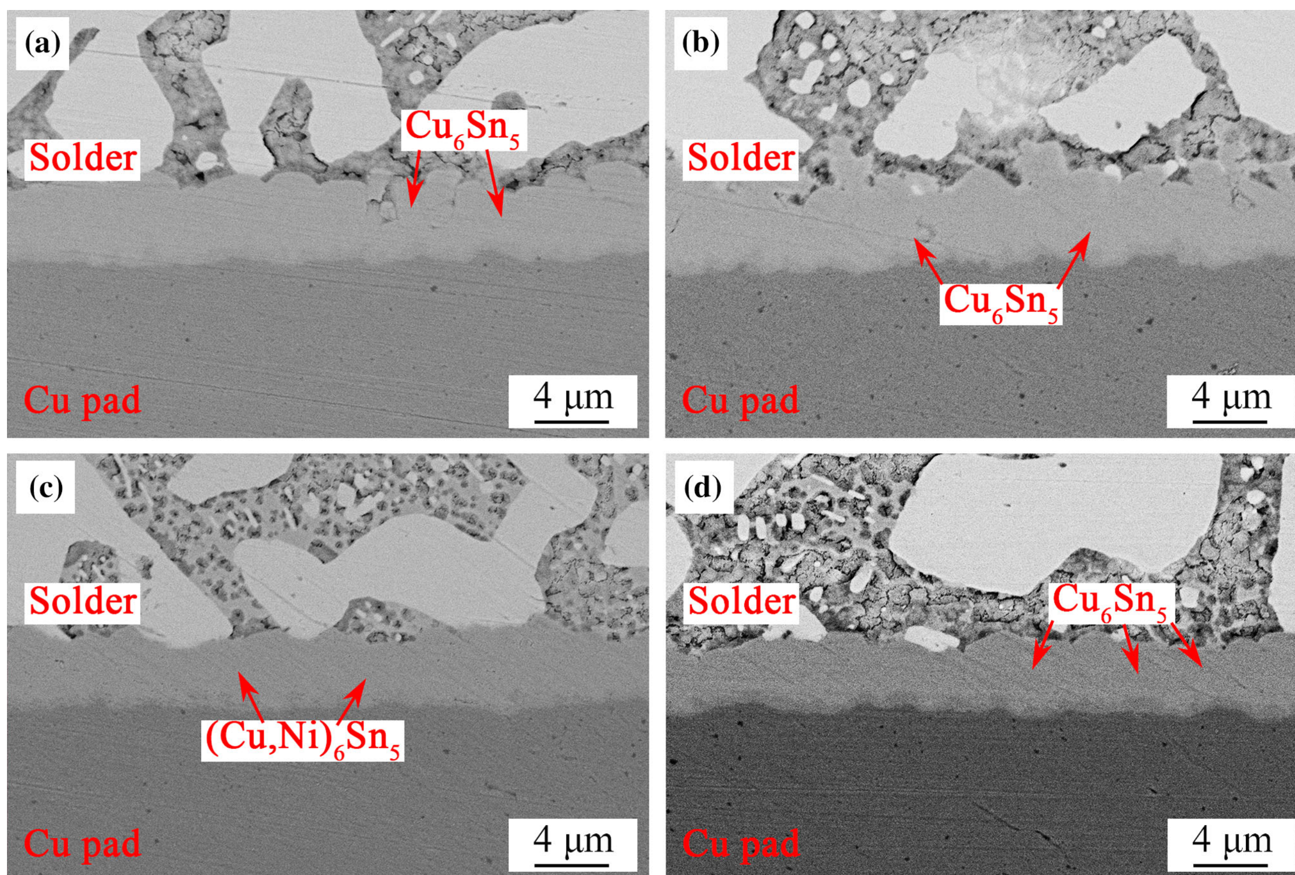

Fig. 9 The interface SEM images of SnBi/Sn-Ag-x/Cu solder joints after 700 thermal cycles, **a** SnBi/SAC305/Cu, **b** SnBi/SAC0307/Cu, **c** SnBi/SACBN/Cu, and **d** SnBi/SABI333/Cu

Table 1 The thickness of IMC after thermal cycles

	The thickness of IMC (µm)			
	0 Cycles	300 Cycles	500 Cycles	700 Cycles
SnBi/Cu	0.61 ± 0.03	2.87 ± 0.07	4.07 ± 0.13	5.1 ± 0.09
SnBi/SAC305/Cu	2.64 ± 0.12	3.01 ± 0.06	4.02 ± 0.09	4.29 ± 0.14
SnBi/SAC0307/Cu	2.23 ± 0.08	2.98 ± 0.13	3.15 ± 0.07	4.78 ± 0.11
SnBi/SACBN/Cu	1.72 ± 0.03	3.01 ± 0.03	3.52 ± 0.03	3.85 ± 0.03
SnBi/SABI333/Cu	1.07 ± 0.05	2.83 ± 0.15	3.52 ± 0.16	3.72 ± 0.08

growth of Cu_3Sn IMC is mainly based on the interaction between Cu atoms and Cu_6Sn_5 in the high-temperature stage of the thermal cycles.

Figure 8 presents the interfacial IMC morphologies of SnBi/Sn-Ag-x/Cu solder joints. As shown in Fig. 8a–d, the morphology and thickness of the IMC at the SnBi/Sn-Ag-x/Cu solder joint interface are varying due to the different compositions of the Sn-Ag-x solder leveling layers. Figure 9 shows the interfacial SEM images of SnBi/Sn-Ag-x/Cu solder joints after 700 thermal cycles. The variation of IMC thickness at the interface is similar to that of the SnBi/Cu solder joints. As the number of cycles increases, the interfacial IMC thickens along the solder direction. At the same time, the shape of IMC gradually turns from scalloped to flat. However, during thermal cycling, there is almost no Cu3Sn on the interface IMC of SnBi/Sn-Ag-x/Cu solder joints, indicating that the growth rate of Cu_3Sn is slower

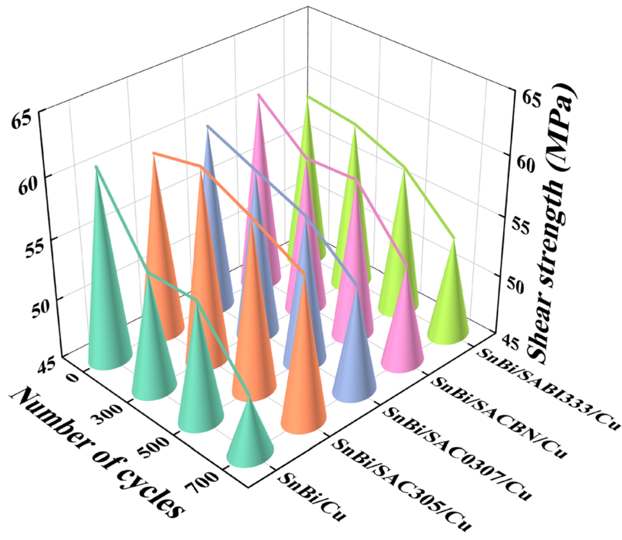

Fig. 10 Effect of thermal cycling on shear strength of solder joints

than that of SnBi/Cu solder joints. Compared with SnBi solder joints, SnBi/Sn-Ag-x/Cu solder joints also suppress the aggregation of Bi at the interface during thermal cycling.

The total IMC thickness of different solder joints after thermal cycling was calculated by Photoshop software, as shown in Table 1. The interfacial IMC thickness of the five solder joints increases with thermal cycling. Although the interfacial IMC of solder joints with Sn-Ag-x leveling layer before cycling is thicker than that of SnBi/Cu solder joints, the IMC thickness of each solder joint is close after 300 cycles. After 700 thermal cycles, the total interfacial IMC thickness of SnBi/Sn-Ag-x/Cu solder joints is lower than that of SnBi/Cu solder joints. The increase in the total thickness of the interfacial IMC layer during thermal cycling mainly attributes to the growth of Cu_6Sn_5 and Cu_3Sn, mainly due to the induced interfacial diffusion caused by the Cu and Sn concentration gradients at the interface [13, 22]. As shown in the table, the IMC thickness of SnBi/Cu solder joint after 700 thermal cycles is 5.1 μm. The thickness of SnBi/SAC305/Cu, SnBi/SAC0307/Cu,

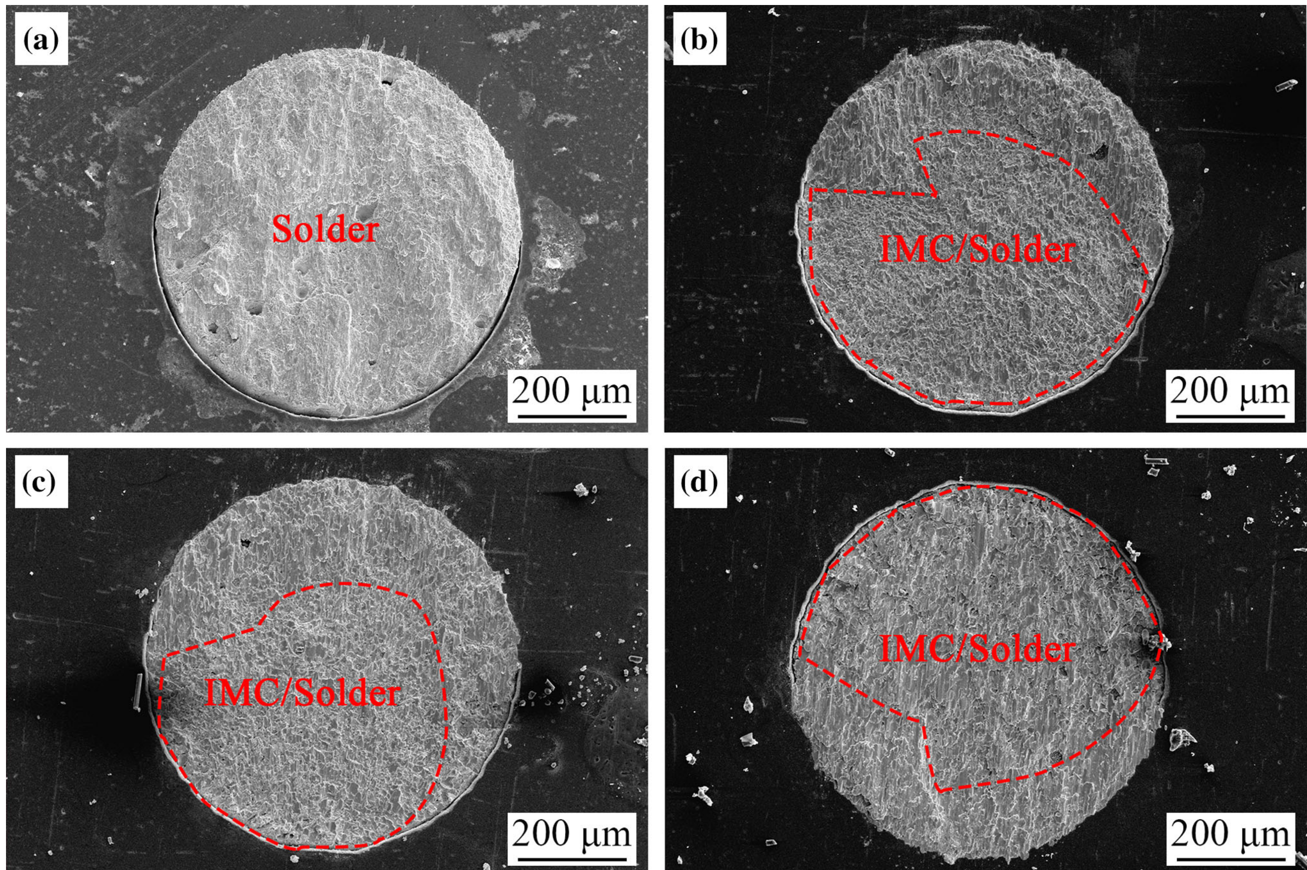

Fig. 11 SEM image of fracture after thermal cycling of SnBi/Cu solder joint, **a** 0 cycles, **b** 300 cycles, **c** 500 cycles, and **d** 700 cycles

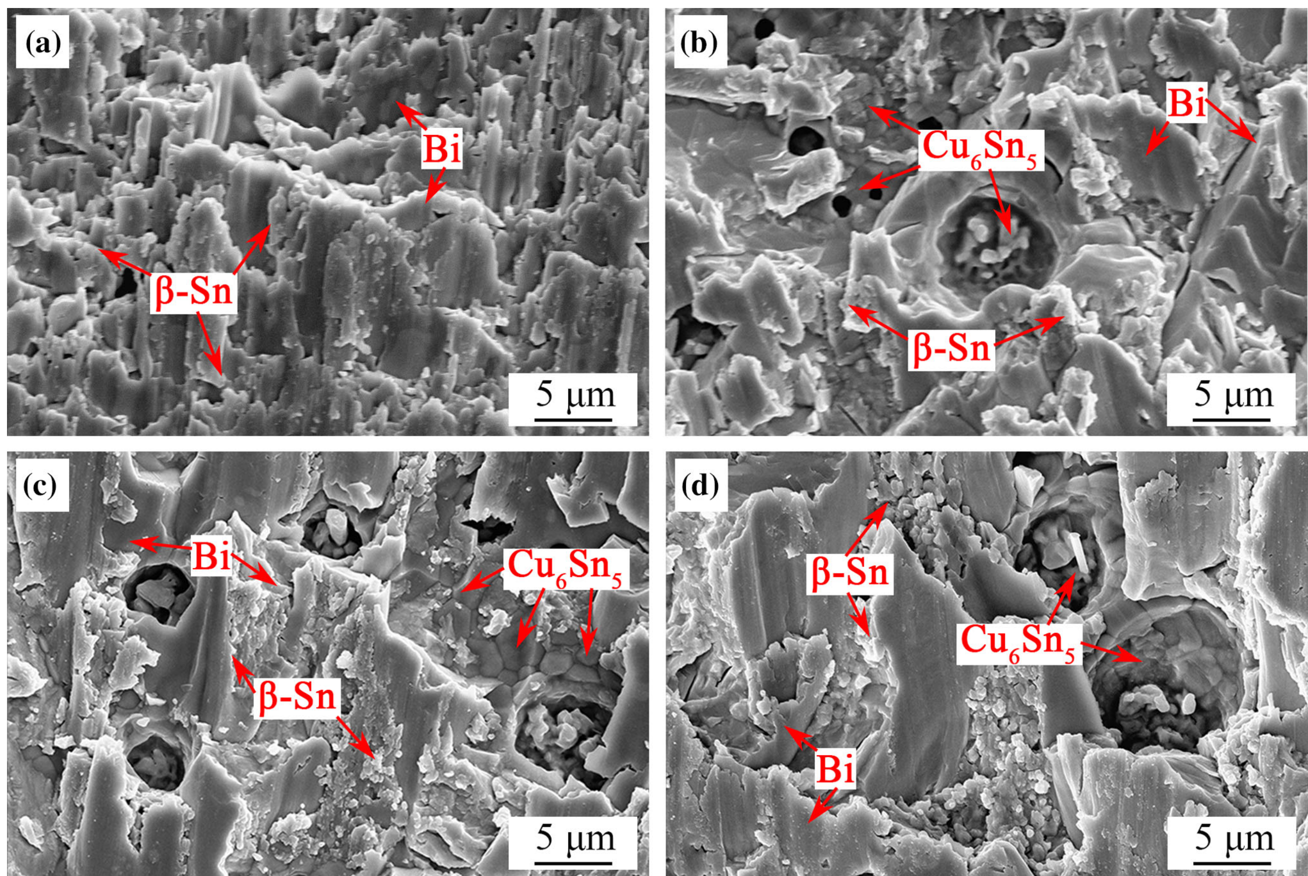

Fig. 12 SEM enlarged image of fracture after thermal cycling of SnBi/Cu solder joint, **a** 0 cycles, **b** 300 cycles, **c** 500 cycles, and **d** 700 cycles

SnBi/SACBN/Cu, SnBi/SABI333/Cu solder joints is 4.29, 4.78, 3.85 and 3.72 μm, respectively. The results show that the Sn-Ag-x leveling layer suppresses the overgrowth of the IMC layer at the SnBi solder joint interface during thermal cycling. According to the previous experimental results, on one hand, the addition of the leveling layer changes the morphology of the interfacial IMC and changes its growth behavior. On the other hand, the melting of the leveling layer changes the microstructure and element concentration of the interface region, which changes the diffusion behavior of the interface and affects the coarsening of the IMC.

3.3 Reliability of solder joints under thermal cycling

Figure 10 shows the shear strength of each solder joint after 0, 300, 500, and 700 thermal cycles. It is obvious from the figure that the shear strength of the five solder joints decreases with thermal cycles increasing. As the number of thermal cycles reaches 300, the shear strength of SnBi/Cu solder joints decreases rapidly. The shear strength of SnBi/Cu solder joints drops significantly from 60.88 MPa to 49.78 MPa after 700 thermal cycles, and the decrease rate reaches 18.23%. The shear strength of SnBi/SAC305/Cu, SnBi/SAC0307/Cu, SnBi/SACBN/Cu and SnBi/SABI333/Cu solder joints decreases to 56.96, 53.78, 53.14 and 53.27 MPa, respectively, which drops by 5.1%, 10.86%, 12.97% and 10.06%, respectively. The addition of the Sn-Ag-x leveling layers inhibits the decrease of shear strength. The mechanical properties of solder joints decrease with the coarsening of microstructure during thermal cycling [23]. In addition, the thickness of the IMC layer is too large and its brittle characteristics decrease solder joint reliability. Therefore, the addition of Sn-Ag-x solder leveling layers improves the shear strength of SnBi solder under thermal cycling, and the shear strength of the SnBi/SAC305/Cu solder joint is the highest after thermal cycling treatment.

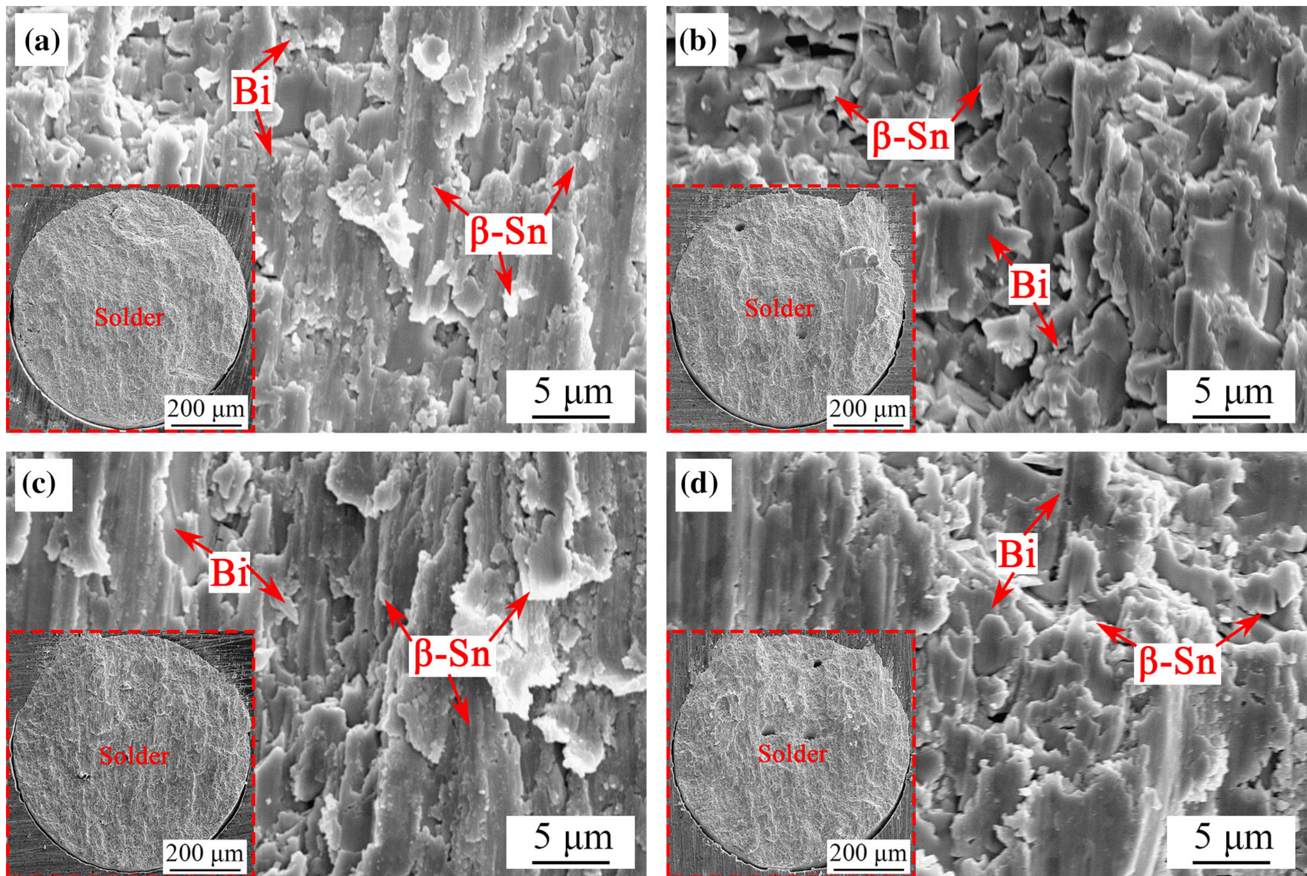

Fig. 13 Fracture SEM images of SnBi/Sn-Ag-x/Cu solder joints, **a** SnBi/SAC305/Cu, **b** SnBi/SAC0307/Cu, **c** SnBi/SACBN/Cu, and **d** SnBi/SABI333/Cu

Figure 11 shows the shear fracture morphologies of SnBi/Cu solder joints after 0, 300, 500, and 700 thermal cycles. As shown in Fig. 11a, the fracture of the SnBi solder joint in the soldered state mainly occurs in the solder matrix. From the magnification of Fig. 12a, the fracture morphology shows a brittle fracture. Figure 11b–d shows that most of the solder joint fractures occur on the interface between IMC and solder, and some occur in the solder matrix after various thermal cycling. The fracture area of solder joints does not increase significantly. Cu_6Sn_5 grains, residual β-Sn blocks, and Bi-rich blocks can be observed at the fracture, as shown in Fig. 12b–d. When the thermal cycling increases from 300 to 500 cycles, the IMC particle size at the interface increases at the high-temperature stage. In addition, as the number of cycles increases, the pore size increases due to the fracture, as shown in Fig. 12b–d. Therefore, the growth of interfacial IMC grains and serious coarsening of microstructure are the main reasons for the sharp decrease in the shear strength of SnBi/Cu solder joints.

The fracture morphologies of the SnBi/Sn-Ag-x/Cu solder joints before and after thermal cycling are shown in Figs. 13 and 14, respectively. The fracture positions of SnBi/Sn-Ag-x/Cu solder joints before and after thermal cycling are all located in the bulk solder, as shown in the overall morphologies of the red box on the left bottom of Figs. 13 and 14. As shown in Fig. 13a–d, the fracture of SnBi/Sn-Ag-x/Cu solder joints before thermal cycling is similar to the fracture mode of SnBi solder joints. The enlarged fracture morphologies after 700 cycles are in Fig. 14a–d. Compared with Fig. 13, the volume of residual Bi-rich and β-Sn phases on the fracture surface increases significantly. Figure 7 indicates that the thermal cycling leads to the IMC growth and Cu_3Sn layer formation, which aggravates the stress concentration. As a result, the shear strength of solder joints decreases sharply, and the fracture path appears at

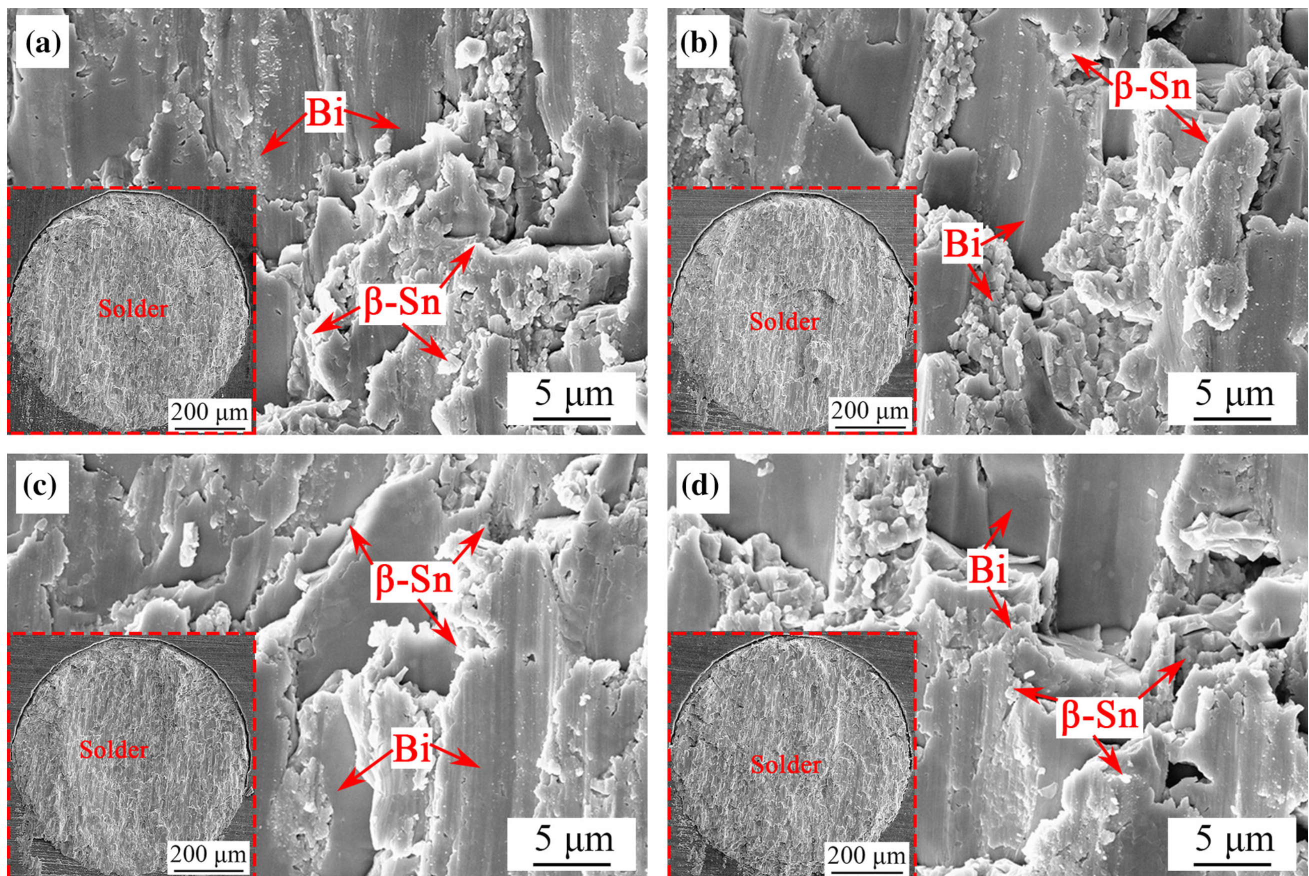

Fig. 14 Fracture SEM images of SnBi/Sn-Ag-x/Cu solder joints after 700 cycles of thermal cycling, **a** SnBi/SAC305/Cu, **b** SnBi/SAC0307/Cu, **c** SnBi/SACBN/Cu, and **d** SnBi/SABI333/Cu

the solder/IMC interface. Therefore, the shear strength of the SnBi/Cu solder joint is lower than that of the SnBi/Sn-Ag-x/Cu solder joint due to the decrease in interfacial strength.

4 Conclusions

1. The microstructure in the five solder joints becomes coarsened with thermal cycles increasing. The grains in the SnBi/Sn-Ag-x/Cu solder joint is more refined than that in the SnBi/Cu solder joints under thermal cycling.
2. The addition of the Sn-Ag-x leveling layer effectively reduces the growth rate of IMC at the soldering interface during thermal cycling and suppresses the formation and growth of Cu_3Sn layer.
3. The shear strength of the SnBi/Cu and SnBi/Sn-Ag-x/Cu solder joints decreases with temperature cycles increasing. The addition of Sn-Ag-x leveling layers effectively improves the shear strength of SnBi solder joints after thermal cycling.

Author contributions

HC: investigation, writing-review & editing. YL: conceptualization, methodology. SZ: investigation, writing-original draft. RC: investigation. YX: supervision.

Funding

The authors declare that no funds, grants, or other support were received during the preparation of this manuscript.

Data availability

The datasets generated during and/or analyzed during the current study are available from the corresponding author on reasonable request.

Declarations

Conflict of interest The authors have no relevant financial or non-financial interests to disclose.

References

1. Y. Liu, B. Ren, Y. Xue, M. Zhou, R. Cao, X. Zeng, Improvement on the mechanical properties of eutectic Sn58Bi alloy with porous Cu addition during isothermal aging. Mater. Res. Express **8**, 076302 (2021)
2. Y. Liu, B. Ren, Y. Xue, M. Zhou, R. Cao, P. Chen, X. Zeng, Pressure-assisted soldering of copper using porous metal-reinforced Sn58Bi solder. J. Mater. Sci. Mater. El **32**, 18968–18977 (2021)
3. P. Yao, X. Li, X. Liang, B. Yu, Investigation of soldering process and interfacial microstructure evolution for the formation of full Cu3Sn joints in electronic packaging. Mater. Sci. Semi. Proc. **58**, 39–50 (2017)
4. L. Sun, L. Zhang, C.C. Wei, M.H. Chen, Y. Zhang, Transient liquid phase bonding (TLPB) of Cu to Cu using Sn interconnect solder reinforced by submicron Al particles. J. Mater. Proc. Tech. **307**(2022)
5. L. Yang, L. Zhu, Y. Zhang, S. Zhou, G. Wang, S. Shen, X. Shi, Microstructure, IMCs layer and reliability of Sn-58Bi solder joint reinforced by Mo nanoparticles during thermal cycling. Mater. Charact. **148**, 280–291 (2019)
6. R. Al Athamneh, D.B. Hani, H. Ali, Reliability modeling for aged SAC305 solder joints cycled in accelerated shear fatigue test. Microelectron. Reliab. **104**, 113507 (2020)
7. Y. Liu, S. Li, W. Song, X. Wang, H. Zhang, F. Sun, Interfacial reaction, microstructure and mechanical properties of Sn58Bi solder joints on graphene-coated Cu substrate. Results Phys. **13**, 102256 (2019)
8. Q. Song, W. Yang, Y. Li, J. Mao, W. Qin, Y. Zhan, Interfacial reaction and mechanical properties of Sn58Bi-XCr solder joints under isothermal aging conditions. Vacuum. **194**, 110559 (2021)
9. F. Wang, L. Zhou, X. Wang, P. He, Microstructural evolution and joint strength of Sn-58Bi/Cu joints through minor Zn alloying substrate during isothermal aging. J. Alloys Compd. **688**, 639–648 (2016)
10. Y. Hirata, C.H. Yang, S.K. Lin, H. Nishikawa, Improvements in mechanical properties of Sn-Bi alloys with addition of Zn and in. Mater. Sci. Eng. A **813**, 141131 (2021)
11. H. Zhang, F. Sun, Y. Liu, Thermal and mechanical properties of micro Cu doped Sn58Bi solder paste for attaching LED lamps. J. Mater. Sci. Mater. El **30**, 340–347 (2019)
12. R. Sun, Y. Sui, J. Qi, F. Wei, Y. He, X. Chen, Z. Sun, Influence of SnO_2 nanoparticles addition on microstructure, thermal analysis, and interfacial IMC growth of Sn1.0Ag0.7Cu solder. J. Electron. Mater. **46**, 4197–4205 (2017)
13. M. Usui, T. Satoh, M. Kamiyama, H. Kimura, Reliability of Cu Nanoparticles/Bi-Sn solder hybrid bonding under cyclic thermal stresses. JOM **73**, 600–608 (2021)
14. J. Depiver, S. Mallik, E. Amalu, Effective solder for improved thermo-mechanical reliability of solder joints in a ball grid array (BGA) soldered on printed circuit board (PCB). J. Electron. Mater **50**, 263–282 (2021)
15. Y. Wang, X.C. Zhao, Y. Liu, Y. Wang, D.M. Li, Microstructure, wetting property of Sn-Ag-Cu-Bi-xCe solder and IMC growth at solder/Cu interface during thermal cycling. Rare Met. **40**, 714–719 (2021)
16. H.W. Miao, J.G. Duh, B.S. Chiou, Thermal cycling test in Sn-Bi and Sn-Bi-Cu solder joints. J. Mater. Sci. Mater. El **11**, 609–618 (2000)
17. H. Lee, C. Kim, C. Heo, C. Kim, J.H. Lee, Y. Kim, Effect of solder resist dissolution on the joint reliability of ENIG surface and Sn-Ag-Cu solder. Microelectron. Reliab. **87**, 75–80 (2018)
18. F. Wang, D. Li, Z. Zhang, M. Wu, C. Yan, Improvement on interfacial structure and properties of Sn-58Bi/Cu joint using Sn-3.0Ag-0.5Cu solder as barrier. J. Mater. Sci. Mater. El **28**, 19051–19060 (2017)
19. Y. Liu, Y. Xue, M. Zhou, R. Cao, X. Zeng, H. Li, S. Zhang, Effects of Sn-Ag-x leveling layers on the microstructure and mechanical properties of SnBi low-temperature solder joint. Solder Surf. Mt. Tech. **34**, 153–161 (2021)
20. R. Xu, Y. Liu, H. Zhang, Z. Li, F. Sun, G. Zhang, Evolution of the microstructure of Sn58Bi solder paste with Sn-3.0Ag-0.5Cu addition during isothermal aging. J. Electron. Mater. **48**, 1758–1765 (2019)
21. X. Li, F. Li, F. Guo, Y. Shi, Effect of isothermal aging and thermal cycling on interfacial IMC growth and fracture behavior of SnAgCu/Cu joints. J. Electron. Mater **40**, 51–61 (2011)
22. T. Laurila, V. Vuorinen, J.K. Kivilahti, Interfacial reactions between lead-free solders and common base materials. Mater. Sci. Eng. R **49**, 1–60 (2005)

23. J. Cui, K. Zhang, D. Zhao, Y. Pan, Microstructure and shear properties of ultrasonic-assisted Sn2.5Ag0.7Cu0.1RExNi/Cu solder joints under thermal cycling. Sci. Rep. **11**, 6297 (2021)

Publisher's Note Springer Nature remains neutral with regard to jurisdictional claims in published maps and institutional affiliations.

Springer Nature or its licensor (e.g. a society or other partner) holds exclusive rights to this article under a publishing agreement with the author(s) or other rightsholder(s); author self-archiving of the accepted manuscript version of this article is solely governed by the terms of such publishing agreement and applicable law.